26th ABCM International Congress of Mechanical Engineering
November 22-26, 2021. Florianópolis, SC, Brazil

COB-2021-0282
SIMULATION OF THE RELATION BETWEEN THE FLUID MIXTURE ADMITTANCE AND PHASE FRACTION IN A WIRE-MESH SENSOR FOR OIL-WATER FLOW

Hugo Fernando Velasco-Peña
Adriana Bonilla-Riaño
CALPOSALLE, Engineering Faculty, University of La Salle, Colombia
hvelasco@lasalle.edu.co; abonillar@gmail.com

Carlos J. G. Rojas
O.M.H. Rodriguez
Mechanical Engineering Department, Engineering School of Sao Carlos, University of São Paulo, Brazil
oscarmhr@sc.usp.br ; carojas93@gmail.com

Abstract. *A considerable part of the flows present in nature and engineering applications involve the simultaneous motion of materials with more than one thermodynamic phase. The study of these multiphase flows can be conducted from experimental, theoretical, or computational perspectives, but the complexity of the phenomena usually demands a combination of them. One of the measurement techniques used for multiphase flow studies is the wire-mesh sensor (WMS). This is an intrusive imaging device with high temporal frequency and medium spatial resolution. The WMS provides indirect measurements of the phases in a flow exploiting its electrical properties. However, the relationship between the electrical properties and the phase fraction is computed with models designed for sensors with conditions not fulfilled by the WMS. The objective of this work is to study the adequacy of some permittivity models using simulations of a WMS immersed in random oil-water patterns. Thus, the tridimensional electric field over each crossing point of a WMS is simulated using the finite element method. The sensor modeled in the study consists of 10 stainless steel wires with 0.05 mm radius, 10 mm long, 2 mm separation between the wires in the same plane, and a distance between planes of 1.5 mm. The oil-water mixtures were carried out keeping the water as the continuous phase and adding oil droplets between 0.8 and 2 mm of radius for each simulation. Several phase fractions were randomly generated providing enough data to relate the electrical properties to the phase fraction. Five permittivity models were tested and three data-driven relationships between the relative permittivity and the phase fraction were proposed.*

Keywords: *Oil–water flow, Finite element method, Wire-mesh sensor, Permittivity, Conductance.*

1. INTRODUCTION

One of the main fronts of multiphase flow research has been focused in the development and application of measuring techniques to aid in the description of fluid phenomena. Examples of such techniques are high frequency needle probes (Angeli and Hewitt, 2000; Lovick and Angeli, 2004), dual-sensor conductivity probes (Zhao and Lucas, 2011), electrical resistance tomography (Hua *et al.*, 2005), gamma ray densitometry (Kumara *et al.*, 2010) and wire-mesh sensors (Prasser, 2008; Silva *et al.*, 2007). This work is oriented towards the wire-mesh technology which performs well considering its spatial and temporal resolution, cost, and safety. As a flow imaging device, the WMS employs the electrical properties of fluids to provide local measurements of the phase fraction. The WMS is formed by a grid of electrodes that divides a cross-sectional area into small regions filled during the fluid flow. An electrical circuit is designed to quantify the perturbations caused by the fluids and depending on the electrical property measured, two types of WMS can be employed. The conductive method is applied in two-phase flows where there is one non-conductive phase (Prasser *et al.*, 1998), while the capacitive technique exploits differences in the electrical permittivity (Da Silva, 2008). In addition to these approaches, a combined measurement of capacitance and conductance can be applied to extend the WMS to three-phase flows (Velasco, 2016).

Although the WMS does not need any inverse reconstruction algorithm, it still requires the use of models to relate the capacitance or conductance to the phase fraction of the fluids. Different models are available in the literature, but there is no consolidated model for the measurements of a WMS. In the case of mixture permittivity models, most relationships have been designed for particular types of electrodes and some are restricted to specific flow pattern conditions. Previous

studies have evaluated permittivity models on WMS measurements against the phase fraction computed via the quick-closing valves technique (QCVs). Da Silva *et al.* (2011) assessed 4 mixture permittivity models for dispersed and dual continuous flows of oil-in-water using 34 experimental conditions. The Maxwell-Garnett model was the best fit for the fully dispersed patterns while the Logarithmic model performed better for the dual continuous flows. Velasco *et al.* (2013) tested twelve permittivity models using the measurements of a capacitive WMS for oil-in-water dispersed flow. The Maxwell-Garnet and Series model provided the best results for the 20 experimental tests performed, but the errors were substantially large. In a subsequent work, Rodriguez *et al.* (2014) made a parametric analysis of the Power-Law and Maxwell-Garnett models using 64 experimental tests. Although the errors remained large, the Maxwell-Garnett model apparently worked well for all the oil fraction range.

In recent years, simulations have also played an important role in the development and evaluation of the WMS technology. The numerical solution of the electric and fluid flow phenomena have supported the study of topics that would be difficult to investigate only in experimental settings. Prasser and Häfeli (2018) explored the reasons for overshoots in local conductance signals and the adequacy of relation models using a 3×3 WMS. Zhang *et al.* (2019) studied the systematic errors caused by the uniform sensitive volume assumption and some geometrical factors. Similarly, Lee *et al.* (2021) used a 9×9 WMS to compare the pseudo-dynamic process with the behavior considering intrusive effects. These studies have provided a better understanding of the factors that affect the accuracy of the WMS, but most of them were focused on the conductance technique and assumed a linear conversion method for the computation of the phase fractions.

This work explores the relationship between the fluid mixture admittance and the phase fraction in a WMS for oil-water flow. The electrical behavior of the sensor is approximated using the finite element method and the data generated with the simulations consist of the admittance on the central crossing point and the volumes of the fluids inside the region of maximum sensitivity. Several phase fractions of an oil-water mixture are generated using the water as a continuous medium and adding dispersed spheres of oil with random locations and sizes. Using this simulated data, three data-driven models are proposed to improve the WMS accuracy for phase fraction measurements. The data-driven models are built on top of available permittivity relation models, including the permittivity and the conductivity as inputs in the determination of the volumetric phase fractions. The first data-driven model relates the mixture's conductivity and relative permittivity to the β parameter that defines the Power-Law relation model. Similarly, the second data-driven model produces a map between the electrical properties and the parameter u of the Maxwell-Garnett model. Finally, the last data-driven model tries to learn how to combine the phase fractions calculated using the Bruggeman, Bruggeman-Maxwell, Looyenga, Power-Law ($\beta = 0.2$) and Logarithmic models.

2. NUMERICAL EXPERIMENTS AND PERMITTIVITY MODELS

2.1 Wire-mesh simulation using the finite element method

The sensor is simulated solving Maxwell's equations in the frequency domain, considering only non-magnetic materials and using a linear constitutive relation. With this approach the canonical equations describing the electrical behavior are simplified into the following expressions:

$$\nabla \cdot \mathbf{J} = \mathcal{Q}, \tag{1}$$

$$\mathbf{J} = \sigma \mathbf{E} + j\omega \mathbf{D} + \mathbf{J}_e, \tag{2}$$

$$\mathbf{E} = -\nabla V, \tag{3}$$

$$\mathbf{D} = \epsilon_0 \epsilon \mathbf{E}, \tag{4}$$

where $\mathbf{J}$ is the electric current density, $\mathcal{Q}$ is a distributed current source, σ is the electrical conductivity, $\mathbf{E}$ is the electrical field intensity, $\omega = 2\pi f$ is the angular frequency, $\mathbf{D}$ is the electrical displacement, $\mathbf{J}_e$ is an externally generated current density, V is the electric scalar potential, ϵ_0 is the permittivity of vacuum and ϵ is the relative electric permittivity.

The 5×5 WMS is formed by 10 stainless steel wires of 0.5 mm radius and 10 mm of length. Wires in the same plane are 2 mm apart and the vertical distance between transmitter and receiver electrodes is 1.5 mm. Figure 1 illustrates the computational domain defined by a box of 12×12×8 mm^3 and discretized with approximately 925000 tetrahedral elements. Multiphase flow patterns are replicated defining a continuous medium with randomly located spheres of dispersed fluids. Mesh refinement is adopted in the cube of 4×4×4 mm^3 centered at the crossing point, considering that the radius of the spheres is uniformly distributed over the interval $[0.8, 2.0]$ mm.

The dynamic behavior of the sensor is emulated by the activation of the central transmitter electrode, set to a 1 V, while all the other wires remain grounded. Each multiphase mixture is simulated using 50 different frequency samples in a range of 1000 Hz to 5 MHz spaced evenly on a log scale. Table 1 presents the electrical properties adopted, dispersed and continuous media are characterized by their electrical conductivity and relative permittivity, and stainless steel electrical

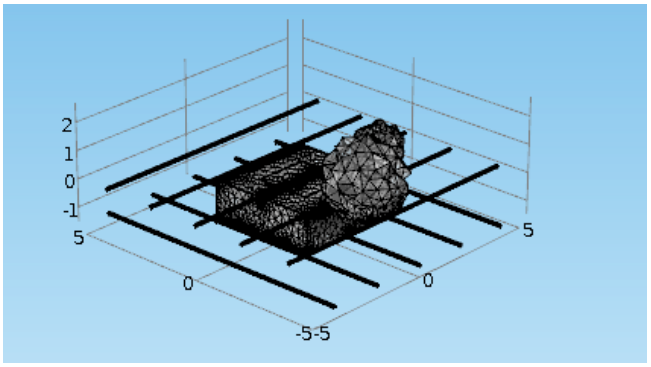

Figure 1. 5×5 WMS simulated.

properties are assigned to the wires. Dirichlet boundary conditions are applied to the top and bottom faces of the domain (voltage set to 0) and Neuman conditions define the boundary on the lateral faces (electric displacement normal to the face, $\mathbf{n} \cdot \mathbf{D}$, set to 0).

Table 1. Electrical properties of the materials used in the simulations.

Material	**Conductivity, σ (S/m)**	**Relative Permittivity, ϵ (-)**
Water	5×10^{-3}	79
Oil	0.04×10^{-15}	3
Steel	6.21×10^{6}	1

After post-processing the results, the final outputs are the admittance at the intersection of the central transmitter and receiver and the volume of the fluids inside the region where the spatial sensitivity is higher. This region is a cube of $d_w \times d_w \times d_w$ centered at the crossing point as suggested by Richter *et al.* (2002) and tested by Da Silva (2008) in his detailed sensitivity study. The admittance is expressed mathematically by the following equation:

$$\mathbf{Y}_x = j\omega k_g \epsilon_0 \epsilon_{\mathbf{x}} = k_g \sigma + j2\pi f k_g \epsilon_0 \epsilon. \tag{5}$$

The term k_g is a constant associated with the sensor that is determined using the electrical properties (conductivity σ and relative permittivity ϵ) of only one fluid. In this case, k_g was calculated using the properties of the water as reference and taking the real or the complex part of the admittance.

The numerical solutions were obtained with a commercial implementation of the finite element method and the different flow patterns were generated using an integration with MATLAB. A parametric function coded in MATLAB creates the oil droplets using a random distribution for the number, size and position of the spheres inside the domain. A total of 309 samples were generated and the distribution of the phase fractions is shown in Fig. 2. It was not observed frequency dependence of the electrical properties, hence the analysis presented in the following sections is independent of the frequency adopted in the simulation.

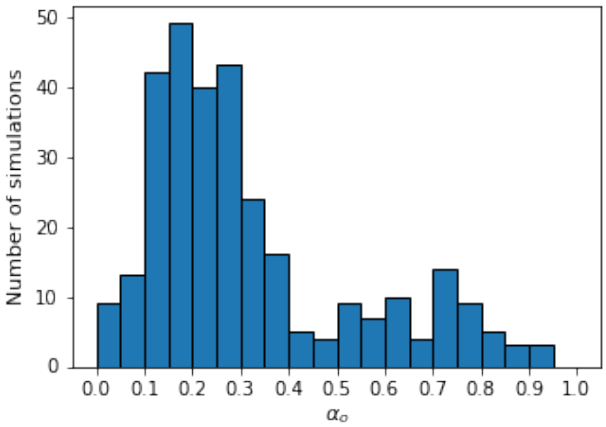

Figure 2. Oil-phase fraction distribution.

2.2 Data-driven permittivity models

Regardless of the technique or circuit used with the WMS, determining the distribution of the fluid requires the application of a relation model to map the electrical properties of the mixture to the volumetric fraction of the fluids. In two-phase flows, only the real (conductance) or complex (capacitance) part of the admittance is necessary, but most relationship models have been developed for the relative permittivity of the mixture. Each relation model was designed for specific sensor geometries, flow patterns and some are considered to be restricted for non-conductive materials. Previous works have sought for an adequate model considering the relationships available in the literature or adjusting parametric models (Velasco *et al.*, 2013; Rodriguez *et al.*, 2014). In this research, three data-driven models are proposed to augment existing permittivity relationships. The first data-driven model relates the mixture's conductivity σ and relative permittivity ϵ_x to the β parameter that defines the Power-Law relation model. The mathematical expression for the volumetric fraction in terms of the Power-Law is given by the expression:

$$\alpha_o = \frac{\epsilon_x^\beta - \epsilon_w^\beta}{\epsilon_o^\beta - \epsilon_w^\beta}, \tag{6}$$

where α_o is the volumetric fraction of oil and ϵ_o, ϵ_w are the relative permittivity of the oil and water, respectively. With this approach, β can assume any value in the range $[0, 1]$ depending on the electrical properties of the mixture. Likewise, the second data-driven model produces a map between the electrical properties (σ, ϵ_x) and the parameter u of the Maxwell-Garnett model. The phase fraction is determined with the Maxwell-Garnett relationship as follows:

$$\alpha_o = \frac{(\frac{\epsilon_x}{\epsilon_w} - 1)(\frac{\epsilon_o}{\epsilon_w} + u)}{(\frac{\epsilon_x}{\epsilon_w} + u)(\frac{\epsilon_o}{\epsilon_w} - 1)}, \tag{7}$$

where $u = 2$ for spheres, $u \to 0$ for discs and $u \to \infty$ for needles, being the water the continuous medium and the oil the dispersed phase. Finally, the last data-driven model tries to learn how to combine the phase fractions calculated using the Bruggeman, Bruggeman-Maxwell, Looyenga, Power-Law ($\beta = 0.2$) and Logarithmic models collected in Tab. 2.

Table 2. Common permittivity relation models available in literature.

Model	Brugemman	Brugemman Maxwell	Series	Parallel	Looyenga	Birchak	Logarithmic
α_o	$\frac{(\epsilon_x+\epsilon_o)(\epsilon_x-\epsilon_w)}{2\epsilon_x(\epsilon_o-\epsilon_w)}$	$(\frac{\epsilon_x-\epsilon_w}{\epsilon_o-\epsilon_w})(\frac{\epsilon_o}{\epsilon_x})^{\frac{1}{3}}$	$(\frac{\epsilon_w-\epsilon_x}{\epsilon_w-\epsilon_o})(\frac{\epsilon_o}{\epsilon_x})$	$(\frac{\epsilon_w-\epsilon_x}{\epsilon_w-\epsilon_o})$	$\frac{\epsilon_x^\beta-\epsilon_w^\beta}{\epsilon_o^\beta-\epsilon_w^\beta}, \beta=\frac{1}{3}$	$\frac{\epsilon_x^\beta-\epsilon_w^\beta}{\epsilon_o^\beta-\epsilon_w^\beta}, \beta=\frac{1}{2}$	$\frac{\log\epsilon_x-\log\epsilon_w}{\log\epsilon_o-\log\epsilon_w}$

Using the data available from the numerical simulations, the determination of the data-driven models is posed as a supervised learning task where the algorithm receives the expected predictions ($\bar{\alpha}_o$) in addition to the features of the models. Furthermore, the training of the β and u models needs to be defined in terms of the Power-Law and Maxwell-Garnett relations because there is no ground-truth reference directly for them. In consequence, neural network models are employed because they make easier to impose these kind of constraints. Neural networks have become very popular due to its successful application in fields such as computer vision and natural language processing, but have also been adopted within different applications in the physical sciences. In particular, the inclusion of physical laws in neural network models (Physics Informed Neural Networks) has been successfully applied for the solution of differential equations and inverse problems (Raissi *et al.*, 2019).

Each neural network acts as a function approximator of one continuous output that can be β, u, or directly α_o. During the training process, the inputs are processed by a block of one or more hidden layers and the output of the network is compared with examples of known predictions $\bar{\alpha}_o$. There are two simple operations applied to each neuron, a weighted sum of all the incoming values followed by a nonlinear transformation which gives the actual output of the neuron. The objective of the training process is to determine the strength of the connections among neurons that reduce the difference between the output of the neural network α_o and the expected prediction $\bar{\alpha}_o$. In a nutshell, a neural network learns patterns useful to map features (inputs) into predictions (outputs). However, it is also necessary to determine the number of layers, neurons per layer, the optimization method, among other settings, that are typically known as hyperparameters. Many recommendations are available for the tunning of these hyperparameters, but in general, their selection is context dependent. An extensive description of how neural networks work and how these hyperparameters are selected is out of the scope of this paper and the authors suggest the following references for an in-depth explanation of the topics (Haykin and Haykin, 2009; Goodfellow *et al.*, 2016; Yu and Zhu, 2020).

Figure 3 depicts an schematic representation of the architectures employed for the parameters' data-driven models. The inputs are the electrical properties (σ, ϵ) and the output of the network is a variable y that represents the β or u parameters of the models. The term f in the figure symbolizes the function of the parametric models (Eq. 6 or Eq. 7).

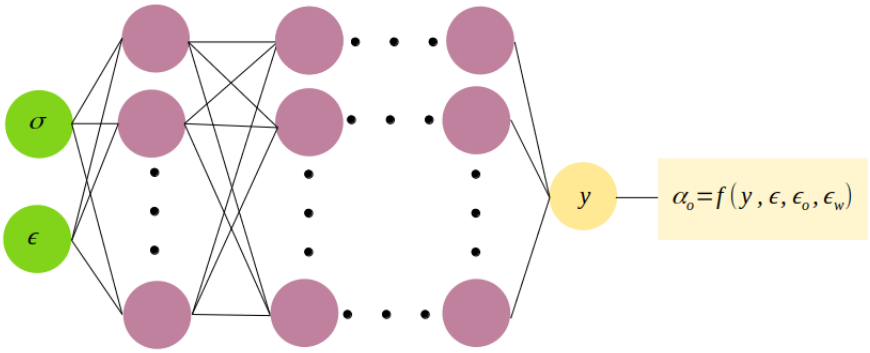

Figure 3. Schematic representation of the neural network models for parameters β and u.

For the third data-driven model (Mix-model) is necessary to add auxiliary inputs with the values of the phase fraction for the Bruggeman, Bruggeman-Maxwell, Looyenga, Power-Law ($\beta = 0.2$) and Logarithmic models. Another difference of the third model in relation to the schematic representation in Fig. 3 is that the output of the network is directly the phase fraction α_o.

3. RESULTS

The neural network (NN) models were implemented using Pytorch (Paszke *et al.*, 2017), an open source machine learning framework, and the hyperparameters were determined using the Optuna optimization software (Akiba *et al.*, 2019). The data obtained with the finite element simulations were divided into training and test sets with a 70-30 ratio (216-93 samples). During the training stage, a cross-validation process was performed to validate the models and tune the hyperparameters. Cross-validation is a resampling procedure commonly used for limited data sets in order to evaluate the performance of the model and avoid overfitting of the data. However, a test set is still necessary because the selection of the hyperparameters is influenced by the performance metric obtained during cross-validation. The hyperparameters considered and the values adopted to define the models are presented in Tab. 3.

Model	Hyperparameter	Best
Mix-NN	Number of layers	10
	Number of units per layer	[7] + [96,52,43,35,31,67,64,67,73,45] + [1]
	Optimizer	Adam
	Learning rate	0.0014
β-NN	Number of layers	7
	Number of units per layer	[2] + [60,57,97,43,34,57,58] + [1]
	Optimizer	Adam
	Learning rate	0.00026
u-NN	Number of layers	4
	Number of units per layer	[2] + [47,29,40,16] + [1]
	Optimizer	AdamW
	Learning rate	0.0038

Table 3. Hyperparameters used in the models.

The first two rows of hyperparameters presented in Tab. 3 define the architecture of the neural networks employed and the last rows are the most important settings for the optimization stage. The number of layers and units per layer is relatively high for all the models and the adaptive optimizers are suitable for noisy problems. In the case of the learning rate, its value determines the amount of change in the model's parameters with regard to the errors in the predictions and depends on the starting point of the model, among others factors. The learning rates adopted prevent a divergence of the training typical of high values, but also avoid long training times caused by too low rates. Another hyperparameter not mentioned in Tab. 3 was the dropout regularization applied to prevent overfitting during the training of the neural network.

Predictions of the oil phase fraction as a function of the relative permittivity are shown in Fig. 4, and the mean absolute percentage errors of the results are illustrated in Fig. 5. Each graphic in Fig. 4 contains the scatter plot of the phase fraction behavior in the test set, the predictions using a neural network, and a relation model that serves as a reference. For the Mix-NN model, the reference is the relationship with less error while the β and u NN results were plotted with the

Power-Law and Maxwell-Garnett predictions, respectively. It can be observed that there are some regions where the NN predictions are not as smooth as the values obtained with the relation models. This behavior is probably due to a trade-off between the regularization of the models and their performance on the validation set.

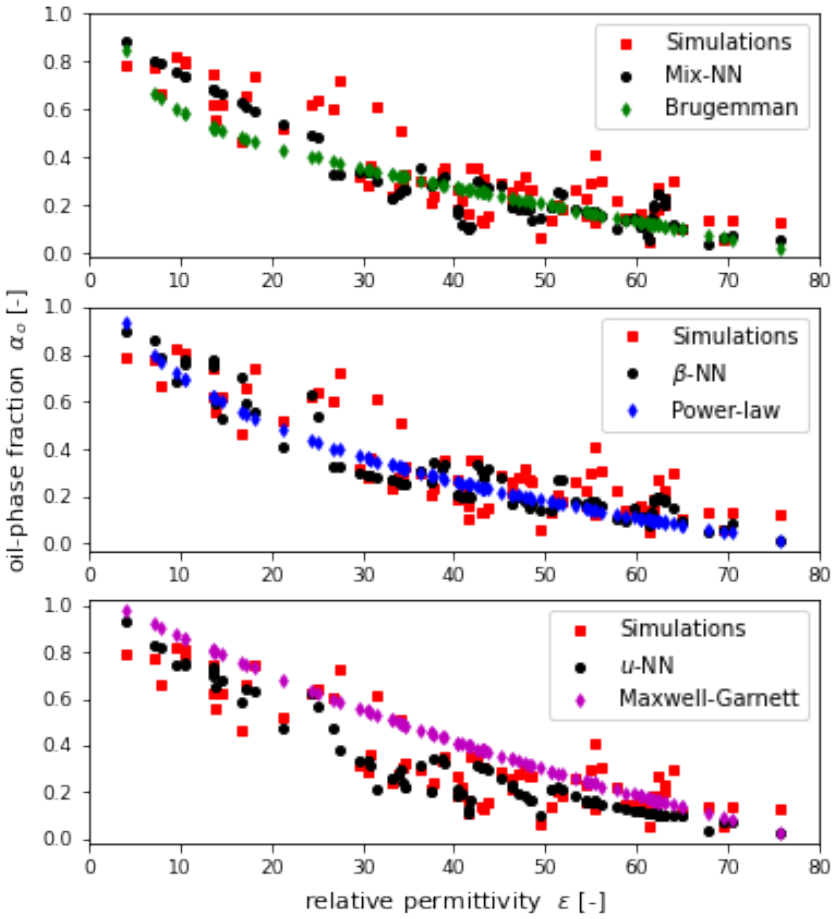

Figure 4. Oil-phase fraction prediction

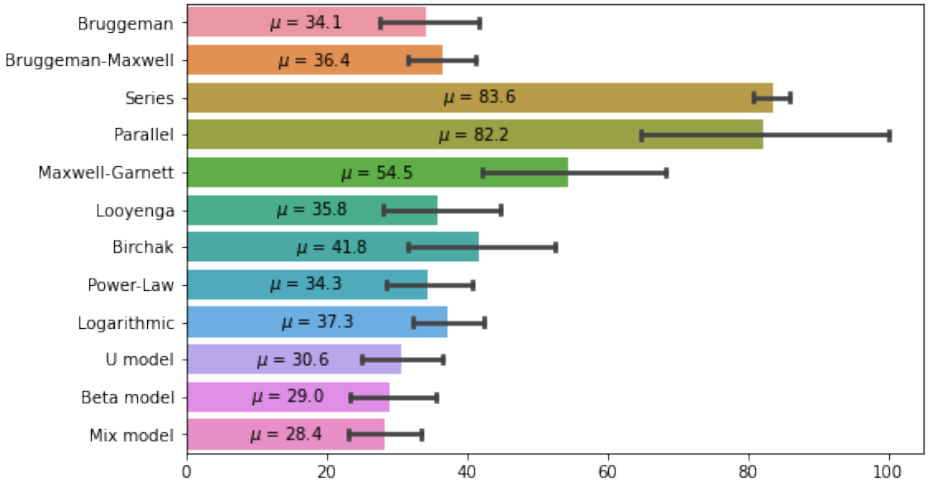

Figure 5. Mean absolute percentage error for each model

Better results of the Mix-NN model in comparison with the Brugemman relationship can be visually attributed to the region with relative permittivities in the range [0,30], where the neural network model gives a better approximation of the phase fraction. In the case of the other graphics, the behavior of the β-NN and the Power-Law (with β = 0.2) models are very similar whereas the phase fractions using the u-NN model are smaller than the Maxwell-Garnett values for almost any relative permittivity value. Figure 5 reveals that the NN models provided better estimations for the phase fractions with acceptable standard deviations. The error using the u-NN model is significantly smaller than the Maxwell-Garnett relation with a fixed $u = 2$ and the errors for the β and Mix models are slightly smaller than the relationships of reference.

4. CONCLUSIONS

In this work was proposed the use of data-driven models to improve the accuracy of phase fraction measurements using a WMS. Two neural network models were trained to relate the electrical properties of the mixture to the parameters of the Power-Law and Maxwell-Garnett relation models. It was also implemented an additional neural network considering the combination of 5 relation models to obtain a better estimation of the volumetric fraction. Although the errors with the data-driven models were slightly smaller than the others, the optimization of the neural network required a significant amount of data for training which can be something difficult to obtain with experiments. Another important point is that the simulations of the WMS were randomly generated without considering any specific pattern for the oil-water mixture and the distributions of the phase fractions were not uniform. This is something to be reconsidered in future works.

5. REFERENCES

Akiba, T., Sano, S., Yanase, T., Ohta, T. and Koyama, M., 2019. "Optuna: A Next-generation Hyperparameter Optimization Framework". *arXiv:1907.10902 [cs, stat]*. ArXiv: 1907.10902.

Angeli, P. and Hewitt, G., 2000. "Flow structure in horizontal oil–water flow". *International Journal of Multiphase Flow*, Vol. 26, No. 7, pp. 1117–1140.

Da Silva, M.J., dos Santos, E.N., Hampel, U., Rodriguez, I.H. and Rodriguez, O.M.H., 2011. "Phase fraction distribution measurement of oil–water flow using a capacitance wire-mesh sensor". *Measurement Science and Technology*, Vol. 22, No. 10, p. 104020.

Da Silva, M.J., 2008. *Impedance sensors for fast multiphase flow measurement and imaging*. Number 33 in Dresdner Beiträge zur Sensorik. TUDpress, Verl. der Wiss, Dresden. ISBN 9783940046994. OCLC: 316204230.

Goodfellow, I., Bengio, Y. and Courville, A., 2016. *Deep Learning*. MIT Press. `http://www.deeplearningbook.org`.

Haykin, S.S. and Haykin, S.S., 2009. *Neural networks and learning machines*. Prentice Hall, New York, 3rd edition. ISBN 9780131471399. OCLC: ocn237325326.

Hua, L., Mi, W., Ying-xiang, W., Yi-xin, M. and Richard, W., 2005. "Measurement of oil volume fraction and velocity distributions in vertical oil-in-water flows using ERT and a local probe". *Journal of Zhejiang University-SCIENCE A*, Vol. 6, No. 12, pp. 1412–1415.

Kumara, W., Halvorsen, B. and Melaaen, M., 2010. "Single-beam gamma densitometry measurements of oil–water flow in horizontal and slightly inclined pipes". *International Journal of Multiphase Flow*, Vol. 36, No. 6, pp. 467–480.

Lee, J.W., Heo, H., Sohn, D.K. and Ko, H.S., 2021. "Development of a numerical method for multiphase flows using an electrostatic model in a wire-mesh sensor". *Engineering Applications of Computational Fluid Mechanics*, Vol. 15, No. 1, pp. 344–362.

Lovick, J. and Angeli, P., 2004. "Experimental studies on the dual continuous flow pattern in oil–water flows". *International Journal of Multiphase Flow*, Vol. 30, No. 2, pp. 139–157.

Paszke, A., Gross, S., Chintala, S., Chanan, G., Yang, E., DeVito, Z., Lin, Z., Desmaison, A., Antiga, L. and Lerer, A., 2017. "Automatic differentiation in pytorch".

Prasser, H.M., 2008. "Novel experimental measuring techniques required to provide data for CFD validation". *Nuclear Engineering and Design*, Vol. 238, No. 3, pp. 744–770.

Prasser, H.M., Böttger, A. and Zschau, J., 1998. "A new electrode-mesh tomograph for gas–liquid flows". *Flow Measurement and Instrumentation*, Vol. 9, No. 2, pp. 111–119.

Prasser, H.M. and Häfeli, R., 2018. "Signal response of wire-mesh sensors to an idealized bubbly flow". *Nuclear Engineering and Design*, Vol. 336, pp. 3–14.

Raissi, M., Perdikaris, P. and Karniadakis, G., 2019. "Physics-informed neural networks: A deep learning framework for solving forward and inverse problems involving nonlinear partial differential equations". *Journal of Computational Physics*, Vol. 378, pp. 686–707.

Richter, S., Aritomi, M., Prasser, H.M. and Hampel, R., 2002. "Approach towards spatial phase reconstruction in transient bubbly flow using a wire-mesh sensor". *International Journal of Heat and Mass Transfer*, Vol. 45, No. 5, pp. 1063–1075. ISSN 00179310.

Rodriguez, I., Velasco, H., Riaño, A., and Rodriguez, O., 2014. "Capacitive wire-mesh sensor measurements in oil-water flow". In *10th International Conference on Heat Transfer, Fluid Dynamics and Thermodynamics*. Orlando, USA.

Silva, M.J.D., Schleicher, E. and Hampel, U., 2007. "Capacitance wire-mesh sensor for fast measurement of phase fraction distributions". *Measurement Science and Technology*, Vol. 18, No. 7, pp. 2245–2251.

Velasco, H., Riaño, A., Rodriguez, I.H. and Rodriguez, O., 2013. "Evaluation of permittivity models for holdup measurements of viscous-oil in water dispersed flow". In *Proceedings of the 4th International Conference on Multiphase Flow*. Jeju, South Korea.

Velasco, H.F., 2016. *Estudo topológico de escoamento trifásico óleo-água-ar através de sensor de impedância de resposta rápida do tipo "wire-mesh"*. Doutorado em Térmica e Fluidos, Universidade de São Paulo, São Carlos.

Yu, T. and Zhu, H., 2020. "Hyper-Parameter Optimization: A Review of Algorithms and Applications". *arXiv:2003.05689 [cs, stat]*. URL `http://arxiv.org/abs/2003.05689`. ArXiv: 2003.05689.

Zhang, H., Xiao, Y. and Gu, H., 2019. "Numerical investigations of the accuracy of conductivity wire-mesh sensors". *Nuclear Engineering and Design*, Vol. 345, pp. 148–156.

Zhao, X. and Lucas, G.P., 2011. "Use of a novel dual-sensor probe array and electrical resistance tomography for characterization of the mean and time-dependent properties of inclined, bubbly oil-in-water pipe flows". *Measurement Science and Technology*, Vol. 22, No. 10, p. 104012.

6. RESPONSIBILITY NOTICE

The authors are solely responsible for the printed material included in this paper.